ISSN 1069-3513, Izvestiya, Physics of the Solid Earth, 2008, Vol. 44, No. 4, pp. 275–290. © Pleiades Publishing, Ltd., 2008.
Original Russian Text © A.A. Lyubushin, 2008, published in Fizika Zemli, 2008, No. 4, pp. 17–34.

Microseismic Noise in the Low Frequency Range (Periods of 1–300 min): Properties and Possible Prognostic Features

A. A. Lyubushin

Schmidt Institute of Physics of the Earth, Russian Academy of Sciences (RAS), Bol'shaya Gruzinskaya ul. 10, Moscow, 123995 Russia

Received September 10, 2007

Abstract—The paper generalizes the experience accumulated in studies of microseismic noise in the period range from 1 to 300 min observed during time intervals preceding a few strong earthquakes. This frequency range is the least studied and occupies an intermediate position between low frequency seismology and investigations of slow geophysical processes. The range includes oscillations induced by atmospheric and oceanic processes and various modes of the Earth's free oscillations excited by very strong earthquakes. The main attention in the paper is given to the background behavior of microseisms, which contains continuous present arrivals from near weak and far strong and moderate earthquakes. The paper focuses on the examination of synchronization effects arising in joint multivariate analysis of information from several stations with estimation of multifractal spectra of singularity and multidimensional spectral measures of coherent behavior of singularity spectral parameters. The problem of using the synchronization effects of microseismic background in the search for new precursors of strong earthquakes is discussed.

PACS numbers: 91.30.Bi

DOI: 10.1134/S1069351308040022

INTRODUCTION

Microseismic oscillations in a wide frequency range are one of the most widespread objects of geophysical studies. This is due to their accessibility, the presence of numerous regional and global seismic networks, and the well-developed practice of seismic observations. Even an approximate review of the literature devoted to analysis of microseisms apparently cannot be made. This is particularly true of the analysis of high frequency (HF) microseisms (from 0.01 to 100 Hz and higher, up to seismoacoustic waves). The widespread occurrence of HF microseismic observations is due to the relative simplicity and mobility of instrumentation free from rigid requirements on long-term stability of sensors that can by no means be neglected in problems of low frequency (LF) geophysical monitoring. Therefore, we mention only briefly a few papers in which more comprehensive references can be found. The paper [Pleskach, 1977] is a pioneering study of the spectral composition of HF microseisms. Various aspects of behavior of HF microseismic fields, including time variations of their intensity and phenomena of modulation and synchronization, in relation to the seismic process are considered in [Rykunov et al., 1979, 1998; Tabulevich, 1986; Saltykov et al., 1997]. The analysis of microseismic oscillations was used for solving problems of geoecology [Spivak et al., 1999; Spivak and Kishkina, 2004]. McNamara and Buland [2004] presented results of detailed research into microseismic background of natural and industrial origin in the frequency band 0.01–16 Hz, including the construction of estimators for the temporal (diurnal and seasonal) and spatial distribution of power spectrum properties.

With an increase in the period of microseismic background oscillations studied, the role of atmospheric and oceanic waves as main sources of microseisms becomes predominant. Berger et al. [2004] presented a review of the use of IRIS broadband seismic stations for the study of background microseisms. Microseismic oscillations in the period range 5–40 s were studied by Stehly et al. [2006], who established their oceanic origin. Continuously observed microseismic oscillations at periods of 100–500 s were examined in [Friedrich et al., 1998; Kobayashi and Nishida, 1998; Tanimoto et al., 1998; Tanimoto and Um, 1999; Ekstrom, 2001; Tanimoto, 2001, 2005; Kurrle and Widmer-Schnidrig, 2006]. These oscillations are generated both by weak earthquakes and by processes in the atmosphere, although the atmospheric effects are predominant. In order for earthquakes to be a source of continuously present microseismic oscillations, at least one earthquake with a magnitude of 6 should occur daily to maintain the observed intensity of such oscillations. The cumulative effect of all weak earthquakes estimated from the Gutenberg–Richter recurrence law yields an energy contribution one to two orders smaller than the observed value. The effect of

Table

Station	Longitude, deg	Latitude, deg	Nov. 5–Dec. 5, 1997 $N = 87775$	Sept. 1–25, 2003 $N = 72000$	Sept. 15–Nov. 15, 2006 $N = 177029$
PET	158.653	53.0167	+	+	+
YSS	142.733	46.954	+	+	+
ERM	143.157	42.015	–	$N = 60892$	+
MAJ	138.207	36.5427	–	–	+
MDJ	129.592	44.6164	–	+	+
INC	126.633	37.483	–	+	+
BJT	116.168	40.0183	–	+	+
OBN	36.5687	55.1138	+	+	+

atmospheric processes (movement of cyclones) and oceanic waves generated by them, as well as the impact of the waves on the shelf and coasts, contributes most to the energy of the LF microseismic background.

The origin of an LF seismic hum with a predominant period of 4 min was studied in [Rhie and Romanowicz, 2004, 2006]. A significant correlation was established between the intensity of these oscillations and the storm wave height in oceans, and it was shown that the hum intensity is independent of the Earth's seismic activity: the authors presented an example of a seismically quiet time interval (January 31–February 3, 2000) characterized, however, by anomalously high amplitudes of microseismic background in the vicinity of the 4-min period. As a possible mechanism of excitation of such oscillations, they proposed the perturbation of the gravitational field by high waves resulting in the excitation of LF seismic waves on the seafloor. The main regions of excitation of these oscillations are suggested to be the northern Pacific Ocean in winter and the southern Atlantic Ocean in summer.

Low frequency oscillations of microseismic background and the Earth's gravitational field with periods of a few tens to a few hundreds of minutes arising due to the lithosphere–atmosphere coupling were considered in [Lin'kov, 1987; Lin'kov et al., 1990; Petrova, 2002; Petrova et al., 2007]. It is important that the source of such oscillations is supposedly slow wavelike deformations of the lithosphere.

The present paper generalizes the experience accumulated in studies of microseismic background in the (LF) range of periods from 1 to 300 min observed in time intervals preceding a few strong earthquakes [Sobolev, 2004; Sobolev et al., 2005; Sobolev and Lyubushin, 2006, 2007; Lyubushin and Sobolev, 2006]. This frequency range is the least studied and occupies an intermediate position between LF seismology and investigations of slow geophysical processes such as gravity field variations, crustal strain and tilt variations, and so on. The range includes various modes of the Earth's free oscillations [Zharkov and Trubitsyn, 1980], excited by very strong earthquakes; however, in the present paper, the main attention is given to the background behavior of microseisms. Note that this background contains continuous arrivals from near weak and far strong and moderate earthquakes.

The joint effect of atmospheric and oceanic processes, tidal deformations of the crust, and the global seismic process, as well as difficultly identifiable and poorly studied processes in the crust related to accumulation and slow dissipation of tectonic energy in the lithosphere, results in a random process the study of which by the traditional tecnique of spectral analysis is ineffective. The methods of identifying periodicities in an event flow, orthogonal wavelet decompositions, estimates of multifractal spectra of singularity, and multidimensional measures of coherent behavior were applied to the study of LF microseismic background in [Sobolev, 2004; Sobolev et al., 2005; Sobolev and Lyubushin, 2006, 2007; Lyubushin and Sobolev, 2006; Lyubushin, 2007].

In this paper, the main emphasis is placed on the study of synchronization effects appearing in a joint multidimensional analysis of information from several stations. The synchronization effects of microseismic background are also examined as a means for detecting new precursors of strong earthquakes.

PROPERTIES OF SCALAR SIGNALS

Initial data of the analysis are broadband continuous seismic records of the vertical component with a discretization frequency of 20 Hz obtained at a few IRIS stations and kindly afforded to the author by the RAS Geophysical Service. To reduce the data set to the LF range, averages were preliminarily calculated in non-overlapping successive intervals 600 samples long. In this way, a transition was performed to a discretization step of 30 s (0.5 min) for which the minimum period available for analysis (the Nyquist period) is equal just to 1 min.

The coordinates of eight IRIS stations whose seismic records are analyzed in the paper are presented in the table, where plus and minus signs are also given for each station to indicate, respectively, the presence and absence of a continuous time series in the time intervals specified in column headings.

The chosen time intervals preceded strong earthquakes: November 5–December 5, 1997, before the Kronotsky earthquake of December 5, 1997 ($M = 7.8$; 54.64°N, 162.55°E); September 1–25, 2003, before the Hokkaido earthquake of September 25, 2003 ($M = 8.3$; 41.81°N, 143.91°E); and September 15–November 15, 2006, before the Simushir, Kurile Islands, earthquake of November 15, 2006 (46.57°N, 153.29°E; $M = 8.2$). The value N in the table is the number of samples with a step of 0.5 min. Seven stations (BJT, INC, MDJ, MAJ, ERM, YSS, and PET) are in the Far East region and relatively near to the epicenters, whereas the station OBN (city of Obninsk) is more than 7000 km away and was chosen as a kind of a reference point of observation in an aseismic region. The time series under study are denoted here as abbreviations of the type PET-2003, which indicates a record obtained at the PET station in the time interval September 1–25, 2003. The sign + for the series ERM-2003 is replaced by the number of samples $N = 60\,892$ because the ERM station (nearest to the Hokkaido earthquake epicenter) was out of operation since September 22, 2003, three days before the event.

Data of 1997 were analyzed in [Sobolev and Lyubushin, 2006; Lyubushin and Sobolev, 2006] not only for the stations PET, YSS, and OBN but also for ARU (city of Arti, the Urals), YAK (city of Yakutsk), and MAG (city of Magadan). Data of these stations are not used here and, therefore, are not included in the table. However, we should note that the sign minus for the stations ERM, MAJ, MDJ, INC, and BJT for 1997 in the table does not mean the absence of continuous observations at these stations, simply implying that data of these stations obtained before the Kronotsky earthquake were not used in the paper.

As an example, Fig. 1 presents typical seismic records (Fig. 1c) reduced to a time step of 0.5 min for the eight IRIS stations in the interval September 15–November 15, 2006, before the Simushir $M = 8.3$ earthquake of November 15, 2006 (Fig. 1b). Because seismic records contain arrivals-related high amplitude variations (Fig. 1a) even after the transition to the 0.5-min step (by an averaging procedure), overly high pulses are truncated in the plots shown. As seen from the plots in Fig. 1c, the signals contain intense LF components (mainly tidal variations) and variations in the mean level, both smooth (trends) and fairly sharp.

The plots in Fig. 1c cannot provide any constraints on LF microseismic noise variations because the latter are dominated by tidal variations and high amplitude peaks associated with arrivals from earthquakes. To remove them, we applied nonlinear threshold wavelet filtering [Mallat, 1998]; i.e., each record was subjected to fast discrete orthogonal wavelet transformation with an optimal basis found from the entropy minimum condition for the distribution of squared wavelet coefficients. Then, wavelet coefficients (about 1% of the total number) having the largest absolute values were set at zero regardless of their detail levels, and the inverse transformation was applied to the remaining coefficients. We remind the reader that the detail level of the order α contains signal components with predominant periods from $\delta t \cdot 2^{\alpha}$ to $\delta t \cdot 2^{(\alpha+1)}$, where δt is the discretization time step. Thus, this procedure eliminates prevailing high-amplitude components regardless of their characteristic period and provides the noise proper. Figure 1d presents plots of the resulting noise corresponding to the plots of complete records shown in Fig. 1c.

Figure 2 shows plots of power spectra of records estimated by the same method in overlapping windows 2880 samples (1 day) wide in the range of periods from 1 to 400 min. The window overlap was chosen to be minimal and depending on the series length, so that the set of overlapping windows covered the entire series under study. The general linear trend was removed in each window and the series window fragment was smoothed with a cosine window (as wide as 0.125 of the main window width) in order to remove the effect of remote frequencies; a modified periodogram was then calculated [Brillinger, 1975]. The periodograms were averaged with different windows for each frequency ω, which yielded values of the average periodogram $I_{XX}(\omega)$. Finally, the periodograms $I_{XX}(\omega)$ were smoothed over frequency using Gaussian kernel functions [Hardle, 1989]; i.e., a spectrum at the frequency ω_0 was estimated by the formula $S_{XX}(\omega_0) = \sum_{\omega} I_{XX}(\omega)\psi(\omega_0 - \omega)/\sum_{\omega}\psi(\omega)$. Here $\psi(\omega) = \exp(-(\omega/r)^2)$ is the Gaussian averaging kernel with the smoothing parameter r and the sum is taken over frequency discretes at a step of $\Delta\omega = 2\pi/L$ (L is the window width expressed as a number of samples). In order to compare power spectra for samples of different lengths, the value of r should be chosen in accordance with the number of resulting overlapping windows and thereby with the total length of the sample. The variance of the spectral estimate is inversely proportional to the number of windows and the radius r, which provides a method for ensuring spectral estimates with the same variance. For the longest time series (the year 2006), this parameter was set equal to 2 steps of the frequency resolution $\Delta\omega$ with 62 windows. For shorter series, it was equal to $4\Delta\omega$ (1997, 31 windows), $4.77\Delta\omega$ (2003, 26 windows, except ERM), and $5.64\ \Delta\omega$ for ERM-2003 (22 windows).

Plots of the estimated power spectra are shown in Fig. 2 on the same logarithmic scale (five orders) of the ordinate axes, although the axes are shifted relative to each other to prevent overlapping of the plots; such a representation enables the comparison of characteristic behavior features as a function of period. Note that the shape of the spectra is quite individual. Period ranges of 1–6, 6–60, and 60–400 min differing in log–log slopes

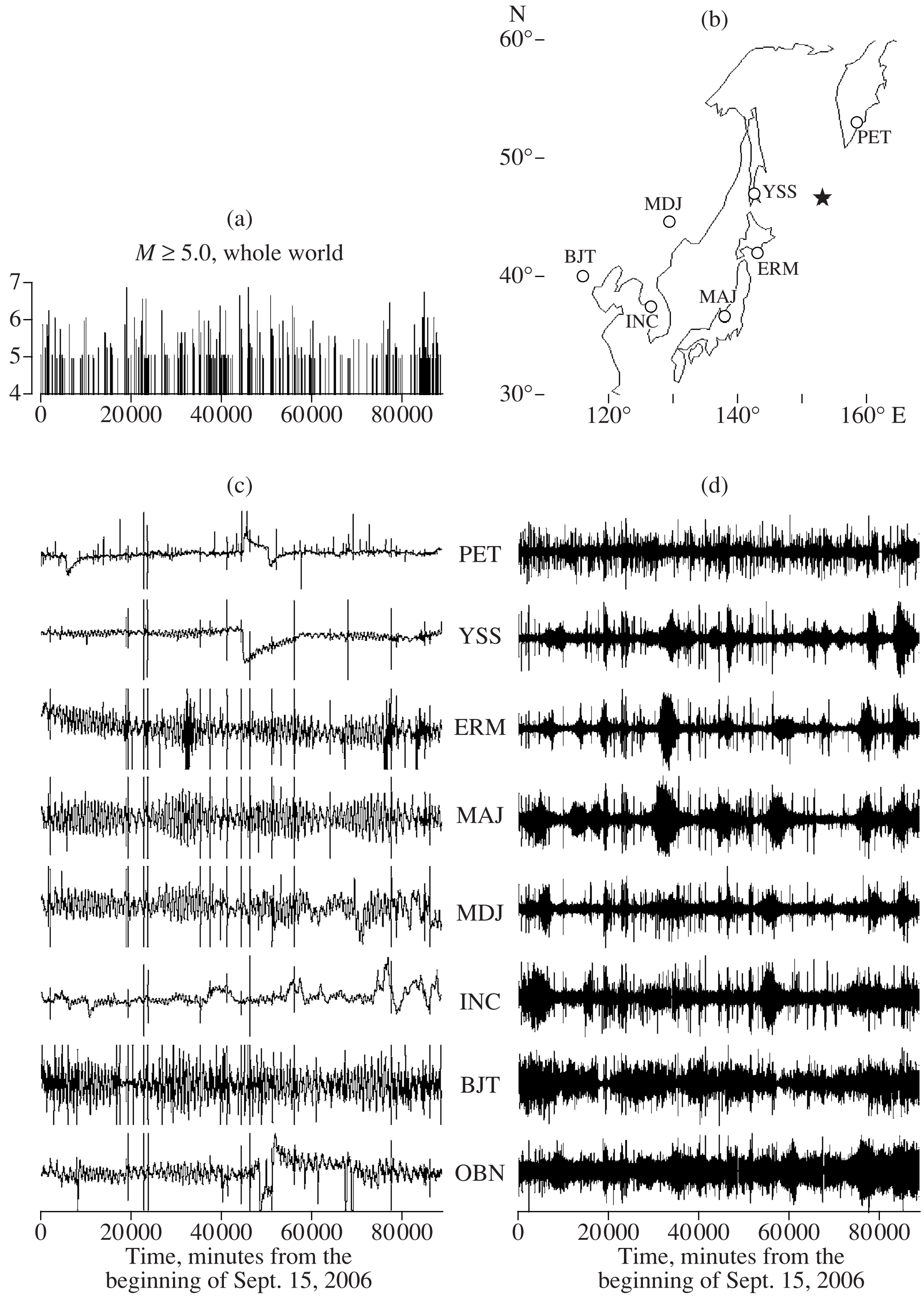

Fig. 1. (a) Sequence of seismic events with a magnitude no less than 5 throughout the world over the time interval September 15–November 15, 2006. (b) Position of stations (circles, except OBN) and the epicenter of the Simushir earthquake of November 15, 2006 (star). (c) Seismic records of eight IRIS stations after the transition to 30-s samples for the time interval from the beginning of September 15, 2006, to 11:13 on November 15, 2006. (d) Noise obtained after threshold wavelet filtering.

(the so-called spectral exponents) are clearly recognizable in the spectra of the MAJ-2006, MDJ-2006, and INC-2006 records and are identified less reliably in the YSS-1997, YSS-2003, and INC-2003 spectra. Another characteristic feature of the plots is that the power spectra of 2006 for periods of 1 to 8 min have a much smaller variance compared to those of 1997 and 2003. This might be due to a larger length of realization, but this cause is removed with the help of stronger (as compared with records of 2006) frequency smoothing of

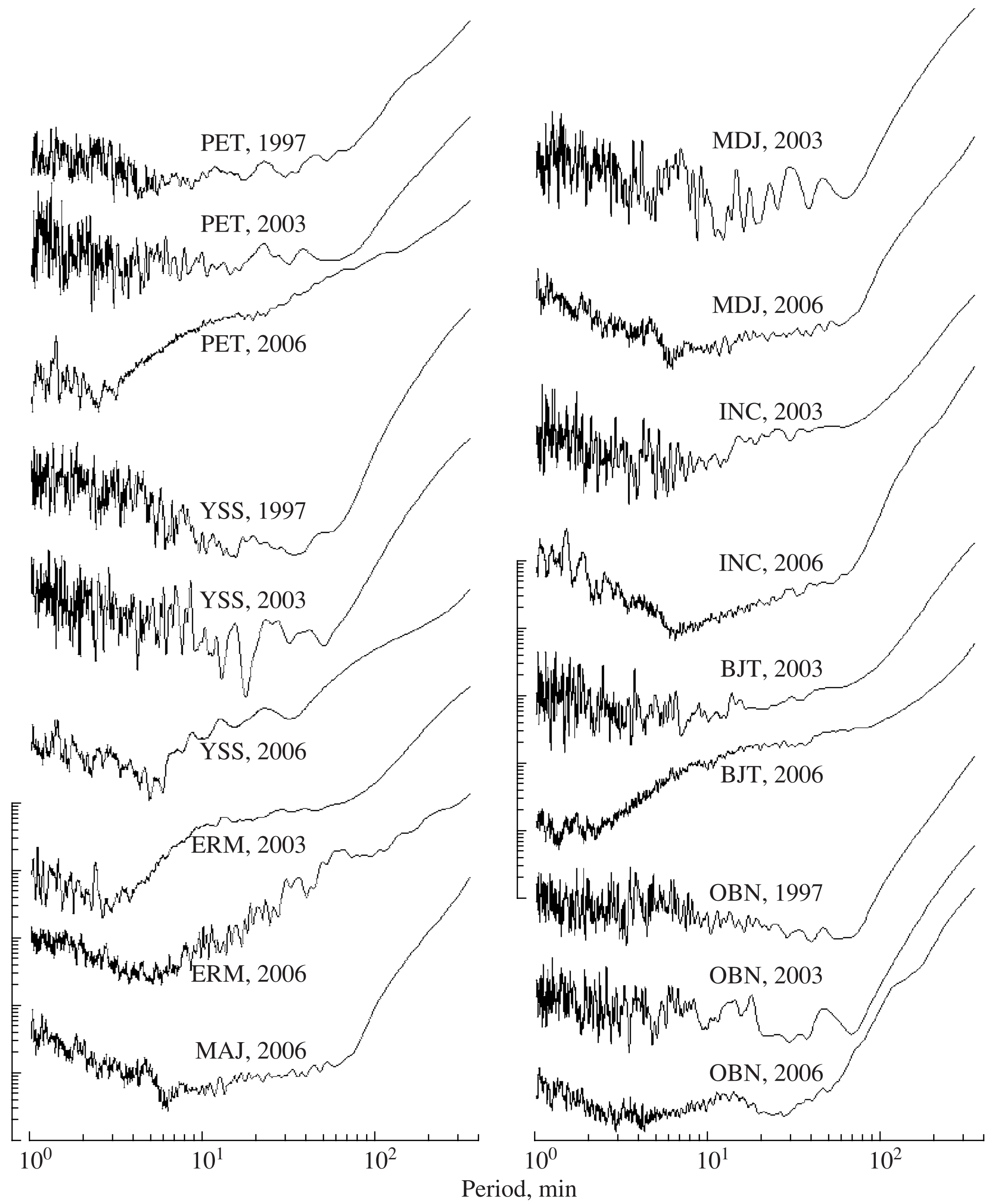

Fig. 2. Plots of power spectra estimated for different stations and in different time intervals. The axes of the plots are shifted relative to each other but have the same logarithmic scale (five orders).

average periodograms for data of 1997 and 2003 by applying the procedure described above. Therefore, it is more likely that this distinction is due to the generation of microseismic oscillations in the lithosphere by high ocean waves in the time intervals of 1997 and 2003. As noted above, this mechanism, generating a macroseismic hum, was investigated in [Rhie and Romanowicz, 2004, 2006]. Thus, the variance rises with an increase in the number of harmonics in a period range of 1–8 min.

A tool effective for the analysis of information is the transition from initial time series to dimensionless integral characteristics of data calculated within a moving time window of a given width. Thus, fractal characteristics such as the Hurst exponent, log–log slope of the power spectrum plot, multifractal singularity spectral parameters, and correlation dimension play an important role in analysis of signals [Hurst, 1951; Feder, 1988; Mandelbrot and Wallis, 1969; Mandelbrot, 1982; Turcotte, 1997]. The analysis of fractal characteristics of monitoring time series is a promising direction in data analysis [Savit and Green, 1991; Currenti et al., 2005; Smirnov et al., 2005; Ramírez-Rojas et al., 2004; Ida et al., 2005; Telesca et al., 2005]. The popularity of the fractal analysis is due to its effectiveness in examining “noises,” i.e., signals that, from the standpoint of spectral theory, are either white noise or Brownian motion. The discovery of the empirical law of Hurst for the case of year-average river runoff [Hurst, 1951; Feder, 1988; Mandelbrot and Wallis, 1969] and its subsequent applications to various random processes in nature, sociology, and finance initiated a wide use of fractal methods in the analysis of time series.

Initially, the Hurst constant H was determined for a time series by the so-called RS-method as a coefficient of linear regression between the values $\ln(RS(s))$ and $\ln(s)$. Here s is the time interval length and $RS(s)$ is the average ratio of the peak-to-valley value of the accumulated sum of deviations from a sample average to the sample estimate of the standard deviation for all time intervals of the length s. In calculating $RS(s)$, the averaging is performed over all intervals of this length lying inside the available sample of the time series. Thus, we have $RS(s) \sim s^H$. We emphasize that these operations should be performed for increments of the time series studied. The empirical law of Hurst states that the value H for a large number of meteorological, hydrological, or geophysical observations is close to 0.7.

The closeness of values of the Hurst constant estimated for different processes is an argument in favor of the fact that they have the same statistical structure, close to properties of self-similar random processes. A random process with continuous time $Y(t)$ is called self-similar with the exponent $H > 0$ if, for any $a > 0$, the distribution function (d.f.) of any finite samples of the random value $Y(a \cdot t)$ coincides with the d.f. of finite samples of the value $a^H \cdot Y(t)$ [Taqqu, 1988]. This means that, if an arbitrary finite number of time moments $t_1, \ldots, t_n$ is changed by a factor of a, the d.f. of the n-dimensional vector with the components $Y(a \cdot t_1), \ldots, Y(a \cdot t_n)$ will coincide with the d.f. of the vector with the components $a^H \cdot Y(t_1), \ldots, a^H \cdot Y(t_n)$. The extension ($a > 1$) or compression ($a < 1$) of the time axis lead, respectively, to an increase or a decrease in the probability of the occurrence of large Y values. In the case of self-similar processes, the same can be achieved by simple extension or compression of the ordinate axis by a^H times. The value H is called a scaling exponent, or the Hurst parameter.

If a self-similar process $Y(t)$ has stationary increments (i.e., for any time step the d.f. of $\Delta_t Y(h) = Y(t + h) - Y(t)$ depends only on h and is independent of t), the succession of the values $z(k) = Y((k+1) \cdot \delta t) - Y(k \cdot \delta t)$ with a fixed time step δt forms a stationary time series with a zero mean. If $0 < H < 1$ and $Y(t)$ is a Gaussian process, $Y(t)$ is called fractal Brownian motion and denoted as $B_H(t)$. If $H = 0.5$, $B_H(t)$ is ordinary Brownian motion, or a Wiener process. Without loss of generality, we may set $\delta t = 1$. If $Y = B_H(t)$, the time series $z(k) = Y(k+1) - Y(k)$, $k = 0, \pm 1, \pm 2, \ldots$, is called fractal Gaussian noise.

The covariance function of fractal noise is described by the formula [Taqqu, 1988]

$$\begin{aligned} \gamma_{zz}(k) &= M\{z(i) \cdot z(i+k)\} \\ &= \sigma^2(|k+1|^{2H} - 2|k|^{2H} + |k-1|^{2H})/2, \end{aligned} \tag{1}$$

where $M\{\cdot\}$ means the mathematical expectation (the mean of the distribution) and $\sigma^2 = Mz^2(k)$ is the variance of the fractal noise ($M\{|Y(t+h) - Y(t)|^2\} = \sigma^2 \cdot |h|^{2H}$). Note that, given $k \neq 0$, $\gamma_{zz}(k) = 0$ (ordinary white noise) if $H = 0.5$, $\gamma_{zz}(k) < 0$ (negative correlation, antipersistence) if $0 < H < 0.5$, and $\gamma_{zz}(k) > 0$ (positive correlation, persistence) if $0.5 < H < 1$. If $H \neq 0.5$, the following asymptotic formula holds:

$$\gamma_{zz}(k) \sim \sigma^2 H(2H-1) \cdot |k|^{2H-2}, \quad |k| \longrightarrow \infty. \tag{2}$$

Let $S_{zz}(\omega) = \frac{1}{2\pi} \sum_{k=-\infty}^{+\infty} \gamma_{zz}(k) e^{-ik\omega}$ be the spectral density of a stationary random sequence $z(k)$. Then, formula (2) implies that $S_{zz}(\omega) \sim \omega^{-(2H-1)}$ as $\omega \longrightarrow 0$; i.e., if $0.5 < H < 1$, $S_{zz}(\omega) \xrightarrow[\omega \to 0]{} \infty$ and the time series $z(k)$ is an LF series.

Now, if the fractal noise is used to calculate its cumulative value, i.e., if the time series $X(k)$ satisfying the relation $X(k+1) = X(k) + z(k)$ is considered, the power spectrum of such a series will formally satisfy the asymptotics $S_{XX}(\omega) \sim \omega^{-(2H+1)}$, $\omega \longrightarrow 0$ and the variance of any realization of such a process N samples long will tend to infinity if N increases by the law $\sim N^{2H}$; i.e., the notion of the power spectrum is strictly speaking inapplicable in the case of the series $X(k)$. It is also evident that many natural processes and, in particular, microseismic background are not self-similar from the standpoint of pure mathematics. However, it is supposed in applied fractal analysis of time series that, in certain time intervals, analyzed signals can possess some properties of self-similar processes and series increments are considered as fractal noise. This implies that characteristics of time series inferred from their fractal analysis are meaningful and can be interpreted (in particular, physically). For example, a finite sample of a series can be used to estimate the power spectrum and determine the log–log slope α of the power spectrum plot as the coefficient of linear regression between $\ln(S_{XX}(\omega))$ and $-\ln(\omega)$ using the formula $S_{XX}(\omega) \sim \omega^{-\alpha}$. The Hurst constant $H = (\alpha - 1)/2$ can then be estimated. This estimate should not necessarily satisfy the condition $0 < H < 1$ and can even be negative but, if it does satisfy this condition, the corresponding time windows can be interpreted as intervals of self-similar behavior.

An alternative method for calculating the spectral component α is the use of the orthogonal wavelet decomposition of signal fragments in the current time window. The Hurst constant can be estimated from the

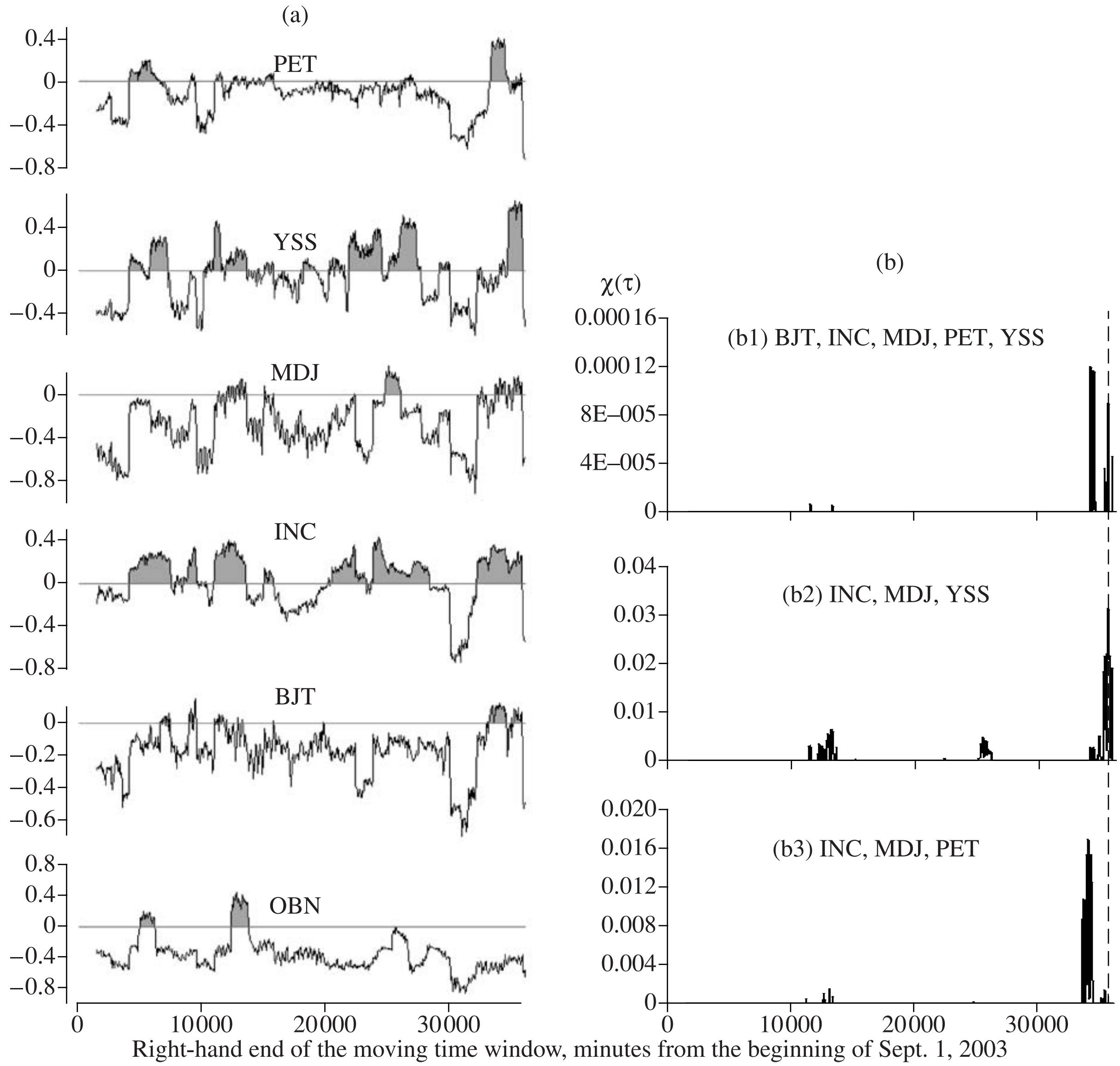

Fig. 3. (a) Variations in the Hurst parameter at the stations indicated in the figure; the parameter was estimated by formula (4) with a moving time window 1 day wide with a shift of 1 h after the removal of the 8th-order polynomial trend in each window. (b1–b3) Variations in value (5) for sets of stations indicated in the figure. The vertical broken line marks the time moment of the Hokkaido earthquake.

increase rate of average squared moduli of wavelet coefficients [Mallat, 1997]:

$$W_k = \sum_{j=1}^{N^{(k)}} \left|c_j^{(k)}\right|^2 / N^{(k)}. \quad (3)$$

Here, $c_j^{(k)}$ is a coefficient of the orthogonal discrete wavelet decomposition of a self-similar time series sample; $k = 1, \ldots, m$ is the number of the decomposition detail level; and $N^{(k)}$ is the number of wavelet coefficients at the detail level k, $N^{(k)} \le 2^{(m-k)}$. Then, by analogy with the relation for the increase rate of a power spectrum, $W_k \sim (s_k)^{2H+1}$, where s_k is the characteristic time scale of the detail level k. As follows from $s_k = 2^k - 2^{(k+1)}$,

$$\log_2(W_k) \sim k^{(2H+1)}. \quad (4)$$

Thus, the slope value of a straight line fitting the pair of values ($\log_2(W_k)$, k) by the least squares method provides an estimate for the value $2H + 1$.

Figure 3a presents the plots of the Hurst constant H estimated after the transition to 30-s time intervals for the data of 2003 (table). The Hurst parameter was estimated with a moving time window 2880 samples (1 day) wide shifted by 120 samples (1 h). To eliminate the effect of tidal variations, a polynomial trend of the

8th order was removed in each window and wavelet power spectrum (3) was calculated for the remainder. For this purpose, we chose an optimal orthogonal Daubechies wavelet with the number of moments set to zero ranging from 2 to 10; this wavelet realizes the entropy minimum for the distribution of squared wavelet coefficients at the first eight detail levels of the wavelet decomposition (scales, or "periods," ranging from 1 to 256 min with a time step of 0.5 min).

Let $H_k(\tau)$ denote the Hurst parameter value estimated for the kth time series as a function of τ, the time coordinate of the right-hand end of the moving window. The values $H_k(\tau)$ obtained for the detrended remainder can be both positive and negative. We are interested in time windows for which these estimates are positive because the Hurst parameter values lie between 0 and 1 in the case of self-similar processes. Therefore, the inequality $H_k(\tau) > 0$ is indirect evidence for fractal self-similar behavior of LF seismic noise. For this reason, it is desirable to identify time windows that yield positive estimates of the Hurst constant for all concurrently analyzed processes, which is evidence for certain LF synchronization. Such windows can identified using the measure

$$\chi(\tau) = \prod_k \max(0, H_k(\tau)). \tag{5}$$

Evidently, value (5) vanishes if the estimate of $H_k(\tau)$ is positive even for one signal.

Figure 3b presents plots of value (5) for different combinations of stations. As a result, we found unexpectedly that the estimates of $H_k(\tau)$ exceeded synchronously the zero level shortly before the Hokkaido earthquake.

The notion of a self-similar process can be further generalized if we assume that the Hurst parameter depends on time, i.e., if we consider a random process such that $M\{|X(t + \delta t) - X(t)|^2\} \sim |\delta t|^{2H(t)}$, $0 < H(t) < 1$. In this definition, one should distinguish between a slow time dependence of the Hurst parameter if it is estimated in a moving time window (evolution) and a "fast" time dependence inside each window considered. The fast dependence of H is related to the notion of the Lipschitz–Holder singularity exponent [Taqqu, 1988; Feder, 1988; Mallat, 1998]. Let $X(t)$ be a certain signal. We define the variability measure $\mu_p(t, \delta)$ of the behavior of the signal $X(t)$ in the interval $[t, t + \delta]$ as

$$\mu_p(t, \delta) = \left(\sum_{s=1}^{s=t+\delta} |X(s)|^p\right)^{\frac{1}{p}}, \quad p \geq 1. \tag{6}$$

In the case of a continuous time, the sum is replaced by an integral.

Note that $\lim\limits_{p \to \infty} \mu_p(t, \delta) = \max\limits_{t \le s \le t+\delta} |X(s)|$; however, in line with Hurst's ideas, we define

$$\mu_\infty(t, \delta) = \max_{t \le s \le t+\delta} X(s) - \min_{t \le s \le t+\delta} X(s); \tag{7}$$

i.e., $\mu_p(t, \delta)$ is the peak-to-valley value of the signal in the time interval $[t, t + \delta]$. The Lipschitz–Holder exponent for the point t is defined as the limit

$$h_p(t) = \lim_{\delta \to 0} \frac{\ln(\mu_p(t, \delta))}{\ln(\delta)}; \tag{8}$$

i.e., the variability measure of the signal $\mu_p(t, \delta)$ in the neighborhood of t decreases by the law $\delta^{h_p(t)}$ with $\delta \longrightarrow 0$. On the strength of formulas (6) and (7), only the right-hand neighborhood of the point t is considered, but this is insignificant for the subsequent manipulations related to the calculation of the singularity spectrum. The singularity spectrum [Feder, 1988; Mallat, 1998] is defined as the fractal dimension of the set of points such that $h_p(t) = \alpha$, i.e., points having the same Lipschitz–Holder exponent equal to α.

The existence of the singularity spectrum is guaranteed only for scale-invariant signals. If $X(t)$ is a random process, we calculate the average value of the measures $\mu_p(t, \delta)$ raised to the power q:

$$M_p(\delta, q) = M\{(\mu_p(t, \delta))^q\}. \tag{9}$$

A random process is called scale-invariant if $M_p(\delta, q)$ decreases by the law $\delta^{\kappa_p(q)}$ with $\delta \longrightarrow 0$, i.e., if there exists the limit

$$\kappa_p(q) = \lim_{\delta \to 0} \frac{\ln M_p(\delta, q)}{\ln(\delta)}. \tag{10}$$

If the dependence $\kappa_p(q)$ is linear, $\kappa_p(q) = H_p \cdot q$, where $H_p = \text{const}$, $0 < H_p < 1$, then the process is called monofractal. In particular, we have $H_p = 0.5$ for the Brownian process. The process $X(t)$ is called multifractal if the dependence $\kappa_p(q)$ is nonlinear.

The operation of raising the measures in (9) to various powers q allows one to assign different weights to time intervals with large and small measures of variability of the signal. If $q > 0$, the main contribution to the average $M_p(\delta, q)$ is made by high-variability time intervals, whereas time intervals with low variability make the largest contribution if $q < 0$.

Note that the use of different exponents p in formula (6) is meaningless in the case of "true" scale-invariant processes (such as the classical multiplicative binomial cascade [Mandelbrot, 1982; Feder, 1988]) because the resulting singularity spectrum is the same. However, in the analysis of real observations, whose properties can either differ strongly from the properties of scale-invariant processes or be similar to them, depending on the time interval processed, the use of different exponents p can lead to different results due to differences in the contribution to measure (6) made by variations in a high amplitude signal with different exponents p. Below, we used three variants: $p = 1$ (the variability measure is the average modulus of deviation), $p = 2$

(the variability measure is the standard deviation), and $p = \infty$ (the variability measure is the peak-to-valley value).

Recently, detrended fluctuation analysis has been widely used for estimating singularity spectra of time series [Kantelhardt et al., 2002]. Below, we briefly describe the main aspects of this method (see also [Lyubushin and Sobolev, 2006; Lyubushin, 2007]).

Let a data sample be divided into nonintersecting intervals s points long:

$$I_k^{(s)} = \{(t\colon 1 + (k-1)\cdot s \le t \le k\cdot s),\ k = 1, \ldots, [N/s]\} \quad (11)$$

and let

$$y_k^{(s)}(t) = X((k-1)s + t), \quad t = 1, \ldots, s \quad (12)$$

be the series fragment $X(t)$ corresponding to the interval $I_k^{(s)}$. If $P_k^{(s,m)}(t)$ is a polynomial of the order m fitting the signal $y_k^{(s)}(t)$ by the least squares method, we consider the deviations from the local trend

$$\Delta y_k^{(s,m)}(t) = y_k^{(s)}(t) - P_k^{(s,m)}(t), \quad t = 1, \ldots, s \quad (13)$$

and calculate the value

$$Z_p^{(m)}(q, s) = \left(\sum_{k=1}^{[N/s]} (\mu_p^{(k)}(s))^q \Big/ [N/s]\right)^{1/q}, \quad (14)$$

which will be considered as an estimate of $(M_p(s, q))^{1/q}$. Here $\mu_p^{(k)}(s)$ is variability measure (6) or (7) of the signal $\Delta y_k^{(s,m)}(t)$ (13) within the interval $I_k^{(s)}$ samples long. The procedure of trend elimination in each small interval s samples long is required if the signal contains trends of external origin (seasonal, tidal, and so on); i.e., it is required to "uncover" noise. We define a function $h_p(q)$ as the coefficient of linear regression between $\ln(Z_p^{(m)}(q, s))$ and $\ln(s)$: $Z_p^{(m)}(q, s) \sim s^{h_p(q)}$. Evidently, $\kappa_p(q) = qh_p(q)$, whereas $h_p(q) = H = \text{const}$ for a monofractal process. In order to account for the possible loss of information at the right-hand end of the sample (if system of intervals (11) covers incompletely the time series fragment analyzed), value (14) is calculated in a similar way on a system of intervals that begins not at the first sample, as in (11), but at the sample next to the last one; the average of values (14) is then taken.

After the function $\kappa_p(q)$ is determined, the next step in the multifractal analysis is the determination of the singularity spectrum $F_p(\alpha)$. Note that the standard approach [Feder, 1988] consists in the calculation of the statistical Gibbs sum $W_p(q, s) = \sum_{k=1}^{[N/s]} (\mu_p^{(k)}(s))^q$ and determination of the mass exponent $\tau_p(q)$ from the condition $W_p(q, s) \sim s^{\tau_p(q)}$, after which the spectrum is calculated by the formula $F_p(\alpha) = \max\{\min_q(\alpha q - \tau_p(q)), 0\}$. Formula (14) readily yields $\tau_p(q) = \kappa_p(q) - 1 = qh_p(q) - 1$. Thus, we have

$$F_p(\alpha) = \max\{\min_q(q(\alpha - h_p(q)) + 1, 0\}. \quad (15)$$

The singularity spectrum is usually calculated by the formula $F_p(\alpha) = q\cdot\alpha - \tau_p(q)$, in which the variable q is replaced by α in accordance with the implicit formula $\alpha = d\tau_p(q)/dq$. Since the function is found numerically, its differentiation is an additional problem. The operation of taking the inner minimum in (15) is much more stable with respect to calculation errors as compared with numerical differentiation. As regards the operation of taking the outer maximum in (15), it is a natural condition (the dimension cannot be negative) for the identification of the singularity spectrum support, i.e., the interval $[\alpha_{\min}, \alpha_{\max}]$ of argument values for which $F_p(\alpha) \ge 0$.

If the spectrum is estimated in a moving time window, its evolution can provide information on the variation in the structure of chaotic pulsations of the series. In particular, noise characteristics are the position and width of the support of the spectrum $F_p(\alpha)$ (the values $\alpha_{\min}$, $\alpha_{\max}$, and $\Delta\alpha = \alpha_{\max} - \alpha_{\min}$ and the value α^* maximizing the function $F_p(\alpha)$: $F_p(\alpha^*) = \max_\alpha F_p(\alpha)$). The value α^* can be called a generalized Hurst parameter. In the case of a monofractal signal, $\Delta\alpha$ should vanish (in practice, this means a small value of the support width estimate) and $\alpha^* = H$. As regards the value $F_p(\alpha^*)$, it is equal to the fractal dimension of points in the neighborhood of which scaling relation (8) is satisfied. Usually $F_p(\alpha^*) = 1$, but there exist windows for which $F_p(\alpha^*) < 1$. We remind the reader that, in the general case (not only in the analysis of time series), the value $F_p(\alpha^*)$ is equal to the fractal dimension of the multifractal measure support [Mandelbrot, 1982; Feder, 1988]. Therefore, the condition $F_p(\alpha^*) < 1$ is interesting as an indicator of a decrease in the dimension of the set of points in the neighborhood of which the noise behavior is governed by the law $M_p(s, q) \sim s^{\kappa_p(q)}$, $s \longrightarrow 0$.

All of the aforementioned parameters of the singularity spectrum are of importance. In the multifractal analysis of time series, main attention is given to the parameter $\Delta\alpha$ of the spectrum support width [Currenti et al., 2005; Ramírez-Rojas et al., 2004; Ida et al., 2005; Telesca et al., 2005] because it directly characterizes the diversity degree of the noise behavior. However, the experience of work with variations in parameters of singularity spectra estimated in relatively short time intervals showed that the generalized Hurst parameter (the value α^*) is least affected by statistical fluctuations. The value α^* characterizes the most typical singularity that is most often encountered within the current window.

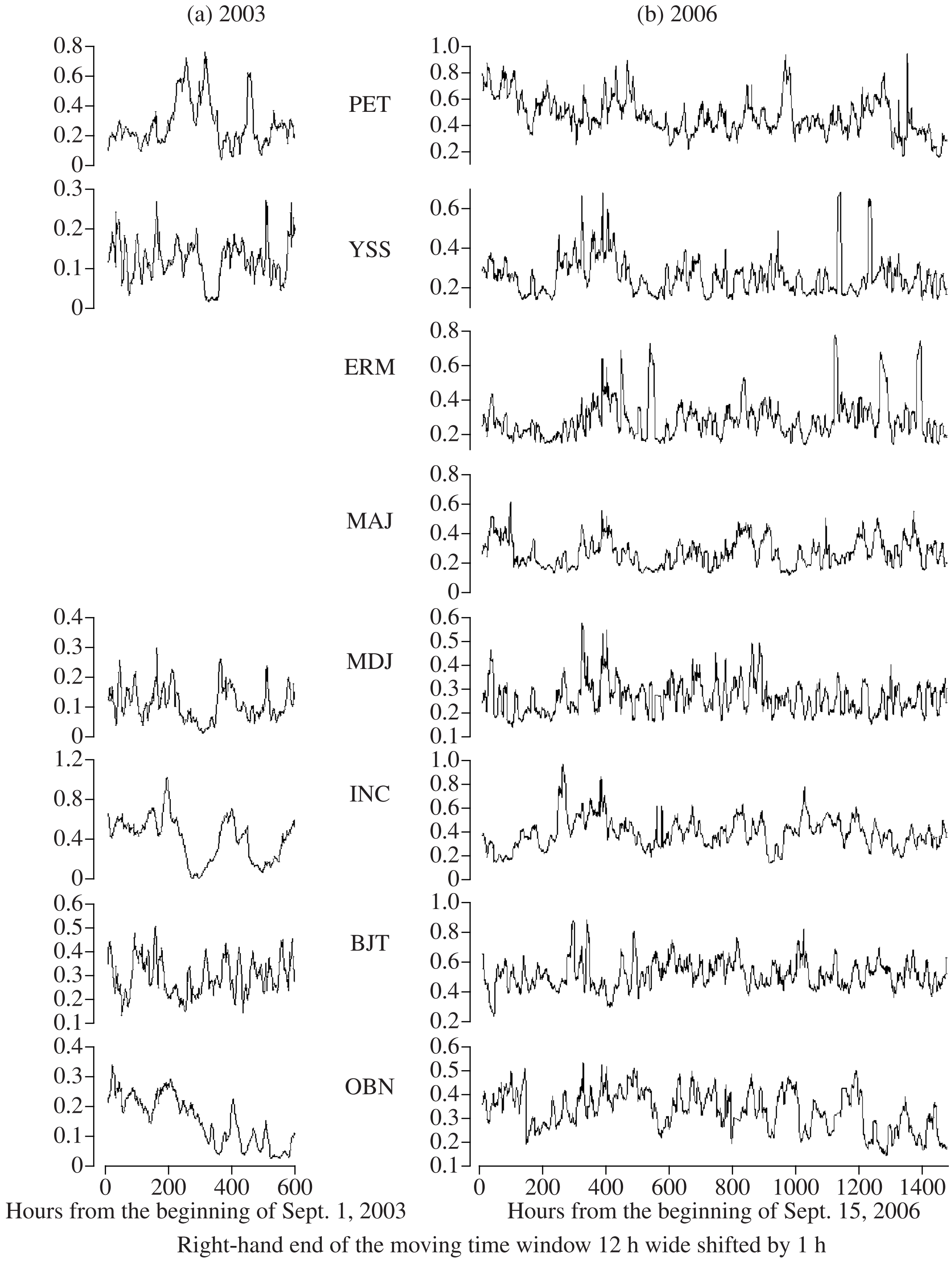

Fig. 4. Plots of variations in α^* for sets of time series of 2003 (a) and 2006 (b); the singularity spectrum was estimated in a moving time window 12 h wide shifted by 1 h.

Therefore, in what follows, the main emphasis is placed on the study of the properties of α^* variations.

Figure 4 presents plots of α^* variations for the sets of time series of 2003 and 2006 (table) obtained by estimating singularity spectra in a moving time window 1440 samples (12 h) wide shifted by 120 samples (1 h). Polynomials of the fourth order were taken to detrend the series by formula (13). The function $h_p(q)$ was estimated in each window for scales varying from a minimum value of 20 samples (10 min) to a maximum value equal to one-fifth of the window width. Given a width of 1440 samples, the maximum scale is 288 30-s samples, or 144 min = 2.4 h. Variability measure (6) with $p = 2$ (standard deviation) was used for the set of series of 2003 and measure (7) (peak-to-valley value) was used for series of 2006.

Thus, the initial time series were replaced by lower frequency series of variations in α^* values (this is why the time axis scales in Fig. 4 are expressed in hours). The goal of the subsequent analysis is the discovery of effects of coherent (synchronous) behavior of LF microseismic oscillations after the reduction of initial data to α^*. The time–frequency structure of peak values of noise exceeding a given threshold and the occurrence of LF asymmetric pulses were studied in [Sobolev, 2004; Sobolev et al., 2005; Sobolev and Lyubushin, 2007] with the help of the method of increments in the logarithmic likelihood function [Lyubushin et al., 1998].

PROPERTIES OF MULTIDIMENSIONAL SIGNALS AND SYNCHRONIZATION

Synchronization effects in behavior of geophysical fields, an increase in their collective component, are an important indicator of changes in the state in the crust and, in particular, precursory phenomena related to strong earthquakes. These effects are treated on the basis of very general patterns of the behavior of systems approaching a bifurcation, or a catastrophe [Nicolis and Prigogine, 1989], for example, an increase in the correlation radius of fluctuations in a neighborhood of the bifurcation point (critical opalescence), which points to a tendency toward synchronism in the entire volume of the system before its transition to a new state. It is very difficult, if at all possible, to give a detailed physical description of the actual synchronization mechanism. This is due to the extreme complexity of the crust and numerous external effects, many of which cannot be measured, and even their presence during the period of observations cannot be established with certainty. Therefore, the use of statistical measures of synchronous behavior for the study of processes preceding strong earthquakes is a means for solving this complicated problem.

Below, the spectral measure of coherence proposed in [Lyubushin, 1998] is used for identifying effects of synchronous behavior in results of measurement of LF microseismic background at several stations. Numerous examples of application of this measure not only in physics of the solid Earth but also in hydrology, meteorology, and climatology are presented in [Lyubushin, 2007], where all technical details of calculations omitted here are given. The spectral measure of coherence $\lambda(\tau, \omega)$ is constructed as the modulus of the product of componentwise canonical coherences

$$\lambda(\tau, \omega) = \prod_{j=1}^{m} |\nu_j(\tau, \omega)|. \tag{16}$$

Here $m \geq 2$ is the total number of jointly analyzed time series (the dimension of a multivariate time series), ω is frequency, τ is the time coordinate of the right-hand end of a moving time window consisting of a certain number of neighboring samples, and $\nu_j(\tau, \omega)$ is the canonical coherence of the jth scalar time series describing the degree of coupling of this series with all other series. The value $|\nu_j(\tau, \omega)|^2$ generalizes the ordinary coherence-quadratic spectrum of two signals to the case when the second signal is a vector rather than a scalar. The inequality $0 \leq |\nu_j(\tau, \omega)| \leq 1$ is valid, and values of $|\nu_j(\tau, \omega)|$ closer to unity point to a stronger linear coupling of the jth series at the frequency ω in a time window with the coordinate τ with analogous variations in all other series. Accordingly, the value $0 \leq \lambda(\tau, \omega) \leq 1$, on the strength of its construction, describes the joint coherent (synchronous, collective) behavior of all signals. Note that the value $\lambda(\tau, \omega)$ belongs to the interval [0, 1] and the closer its value to unity, the stronger the coupling between variations of the components of the multidimensional time series at the frequency ω for the time window with the coordinate τ. We should emphasize that the comparison of absolute values of the statistic $\lambda(\tau, \omega)$ is possible only for the same number of concurrently processed time series because, according to formula (16), with an increase in m the value λ decreases as the product of m values smaller than unity. If only two time series are considered ($m = 2$), function (16) becomes an ordinary coherence-squared spectrum (the frequency-dependent squared coefficient of correlation).

Further, measure (16) is applied to the analysis of effects of synchronous behavior between time series of variations of generalized Hurst parameters α^* at different stations. To implement this algorithm, an estimate of the spectral matrix should be available for the initial multidimensional series in each time window. Below, preference is given to the model of vector autoregression of the third order [Marple, 1987]. The length of the time window used for obtaining the dependence $\lambda(\tau, \omega)$ was taken equal to 5 days. Since each value of α^* is obtained for a time window 12 h wide shifted by 1 h, the width of the time window required for estimating the spectral matrix is equal to 109 samples because $(109 - 1) \times 1 + 12 = 120$ h = 5 days.

It is noteworthy that there exists an analogue of formula (16) involving, rather than canonical coherences, canonical correlations between wavelet coefficients of orthogonal decompositions of initial signals at different detail levels in the current time window. Thus, we obtain a wavelet measure of synchronous behavior of multidimensional time series components [Lyubushin, 2000, 2002, 2007]. To extract synchronization effects, both spectral and wavelet measures were used in [Sobolev and Lyubushin, 2007]. However, to identify synchronization between time series α^*, we use here only the spectral measure because the inferred results are similar and a time–frequency diagram displays the results in a more compact and clear form as compared with a set of linear plots showing the evolution of the

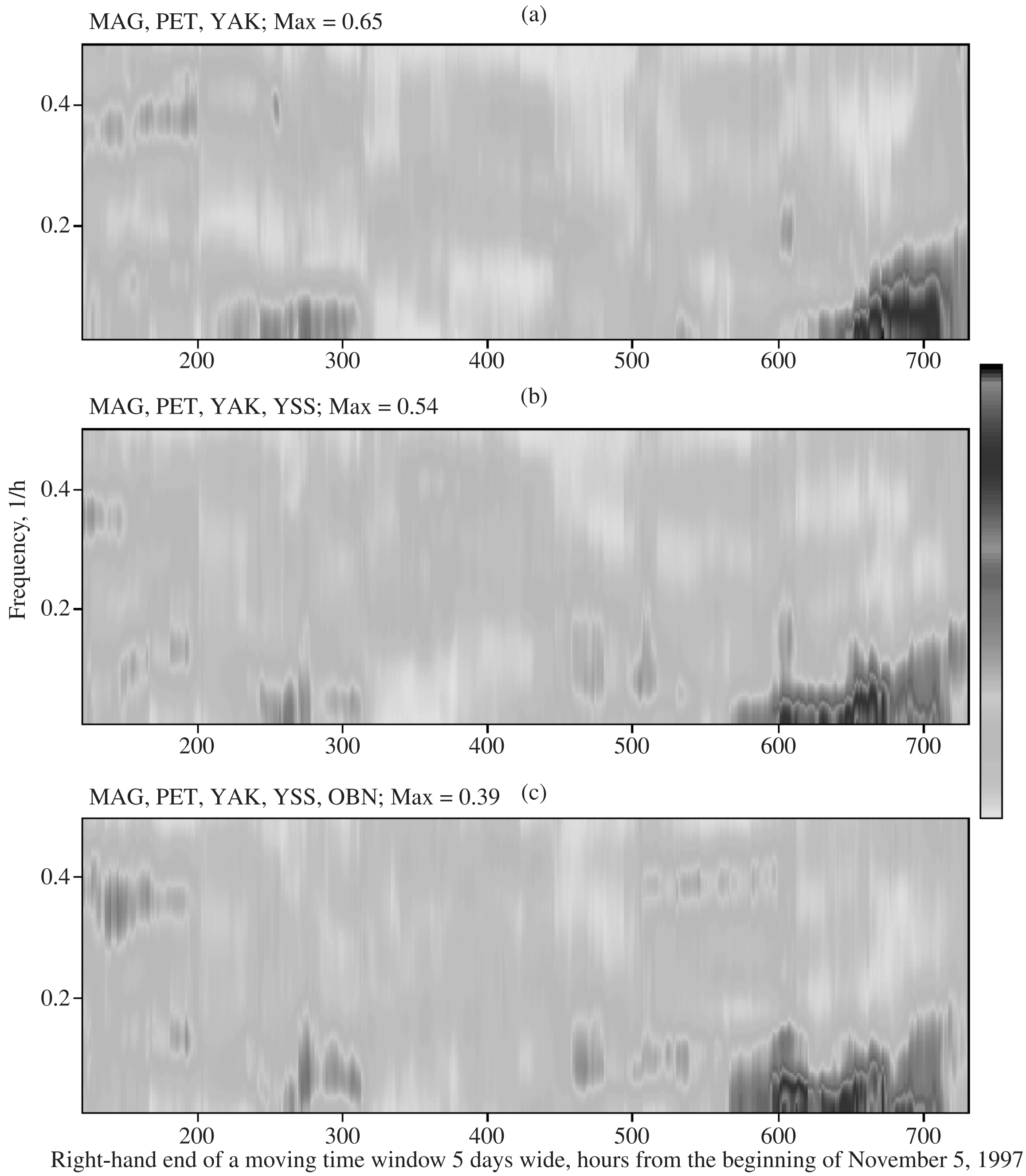

Fig. 5. Time–frequency evolution diagrams of the spectral measure of synchronization for variations in the generalized Hurst parameter α^* of microseismic background before the Kronotsky earthquake of December 5, 1997, after the transition to 0.5-min samples. The parameter α^* was estimated in a moving time window 12 h wide shifted by 1 h. The diagrams show the codes of seismic stations included in the analysis (YAK and MAG stand for Yakutsk and Magadan) and maximum values of statistic (16) (the minimum value is nearly zero for all stations).

wavelet synchronization measure at the detail levels analyzed.

We should note that the direct application of the spectral or wavelet measures to initial seismic records failed to reveal significant synchronization effects except for the trivial synchronization at low frequencies (at periods longer than 2 h), associated with the global tidal response of the lithosphere, particularly in time intervals of observation of intense semidiurnal tides. An exception is the analysis of microseismic background before the Sumatra earthquake of December 26, 2004 (M = 9.2), when synchronization at periods of 20–60 min was supposedly initiated in the vicinity of the epicenter 2.5 days before the catastrophe by the MacQuarie earthquake of December 23, 2004 (M = 7.9)

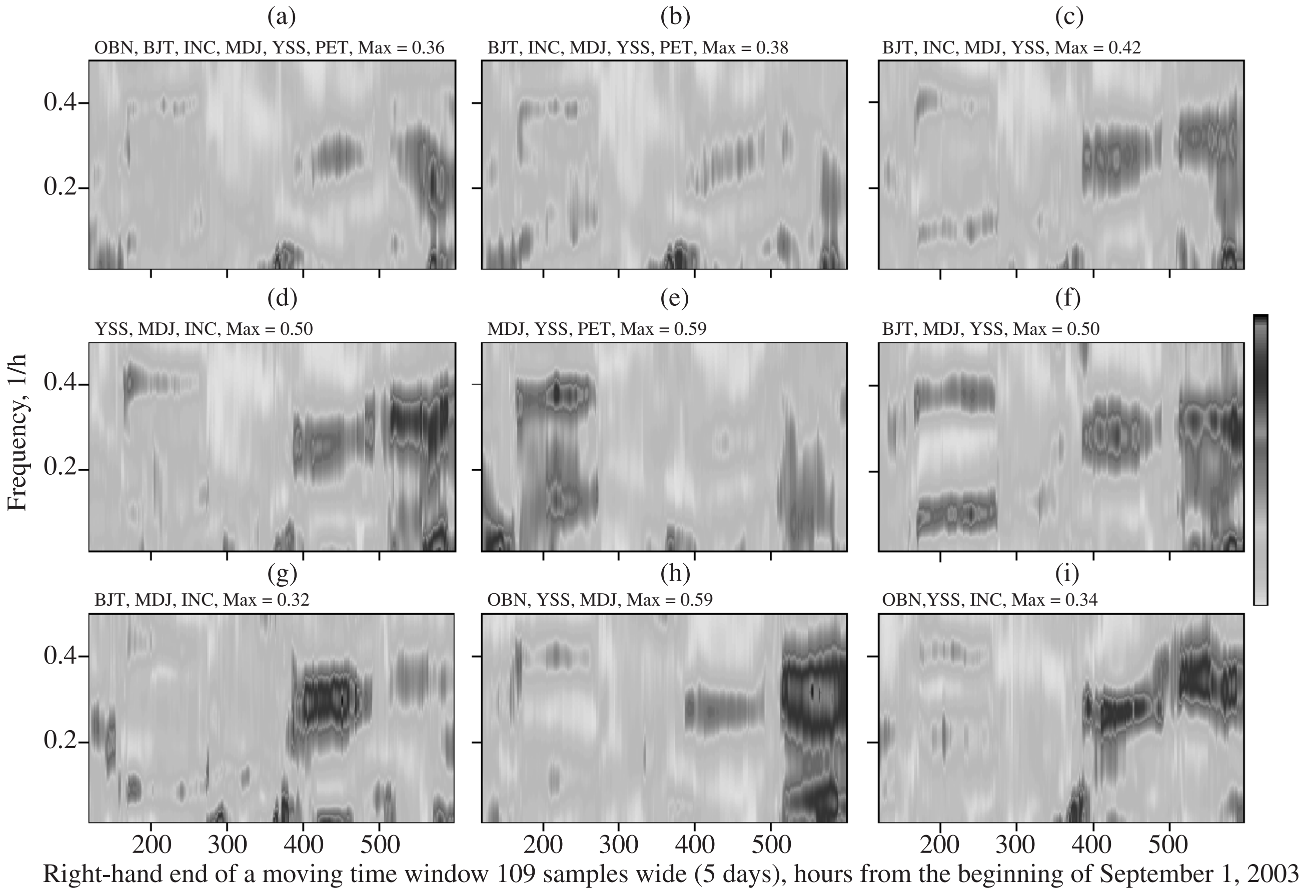

Fig. 6. Time–frequency evolution diagrams of the spectral measure of synchronization for variations in the generalized Hurst parameter α^* of the microseismic background before the Hokkaido earthquake of September 25, 2003, after the transition to 0.5-min samples. The parameter α^* was estimated in a moving time window 12 h wide shifted by 1 h. The diagrams show the codes of seismic stations included in the analysis and maximum values of statistic (16) (the minimum value is nearly zero for all stations).

[Sobolev and Lyubushin, 2007]. However, the transition from initial data to multifractal characteristics within moving time windows allowed us to reveal significant effects of synchronous behavior of the noise characteristics.

Attempts to detect synchronization effects using the ordinary Hurst parameter, i.e., applying measure (16) to time series of the type presented in Fig. 3a, have proven, on the whole, less successful although, for example, the use of measure (5) for records obtained before the Hokkaido earthquake revealed a peak appearing two days before the event (Figs. 3b1–3b3). It was found that the ordinary Hurst parameter is much more sensitive to noises compared to its generalized analogue.

Figure 5 presents results from [Lyubushin and Sobolev, 2006] illustrating the identification of synchronizations between α^* variations before the Kronotsky earthquake. Variability measure (7) (peak-to-valley value) was used for estimating the synchronization spectrum. The diagrams in Fig. 5 display distinct areas of higher values of measure (16) at low frequencies appearing about 3–7 days before the event [Lyubushin and Sobolev, 2006]. There arises a natural question of whether the discovered effect is recognizable in the analysis of information on the LF microseismic field before other strong earthquakes.

Figure 6 shows time–frequency diagrams calculated from statistic (16) for nine different variants of processed stations before the Hokkaido earthquake of September 26, 2003, i.e., for time series of α^* values plotted in Fig. 4a. A stable synchronization, particularly well expressed in Figs. 6c, 6d, 6f, 6h, and 6i, occurs at least 2 days before the event. It is interesting that this synchronization arises rather early (time mark 400 h) but disappears at time mark 500 h, which corresponds to the arrival time interval of waves from two remote strong earthquakes with magnitudes higher than 6. Thus, synchronization of multifractal parameters of seismic background also took place before the Hokkaido earthquake.

However, the expected synchronization effect directly before the Simushir earthquake has not been discovered. Results of the analysis are presented in Fig. 7 also in the form of time–frequency diagrams for various sets of stations; the diagrams were estimated for time

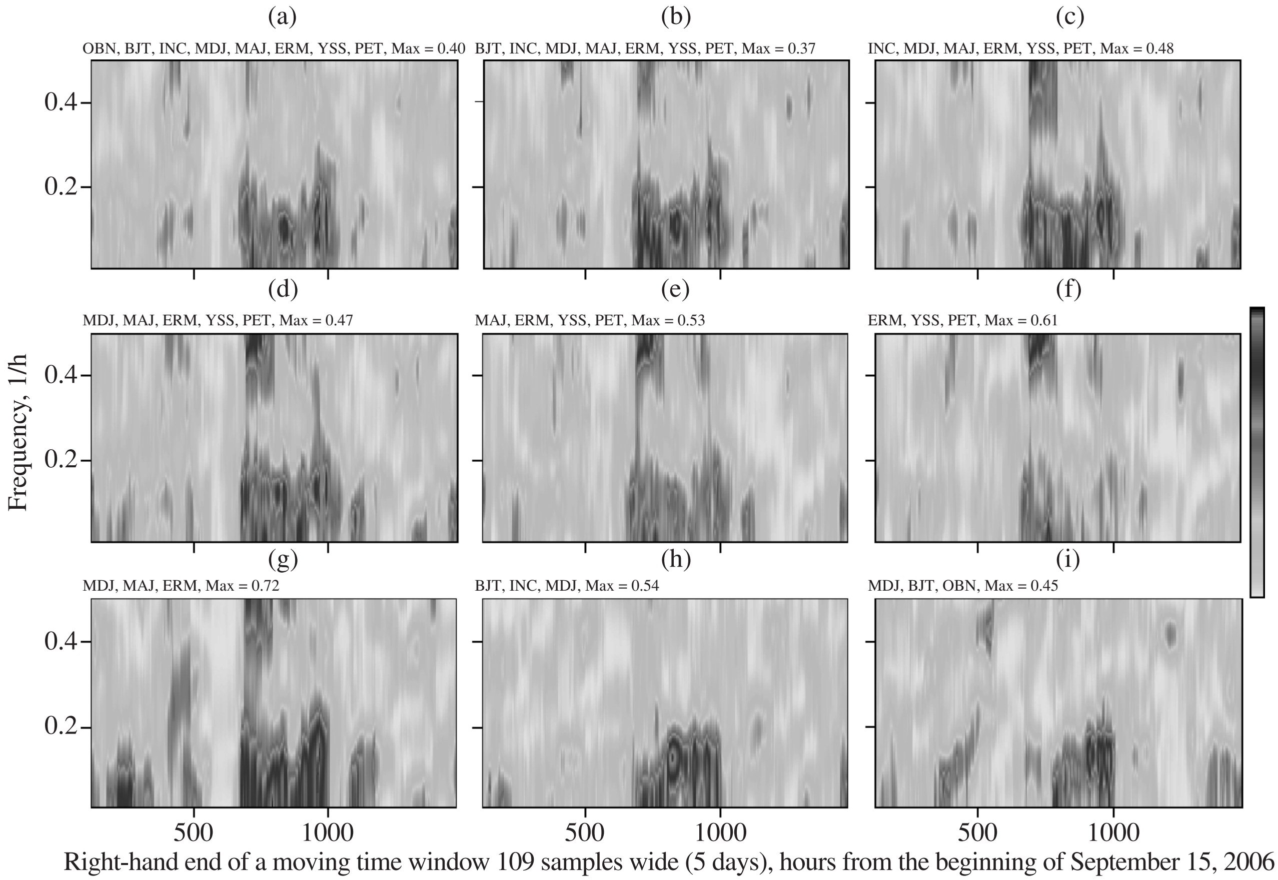

Fig. 7. Time–frequency evolution diagrams of the spectral measure of synchronization for variations in the generalized Hurst parameter α^* of microseismic background before the Simushir earthquake of November 15, 2006, after the transition to 0.5-min samples (Fig. 4b). The parameter α^* was estimated in a moving time window 12 h wide shifted at 1 h. The diagrams show the codes of seismic stations included in the analysis and maximum values of statistic (16) (the minimum value is nearly zero for all stations).

series of α^* shown in Fig. 4b. Moreover, stable absence of synchronization is noticeable before the earthquake; a pulse of synchronous behavior about 16 days long occurred in the middle of the observation interval (October 11–28, 2006), and the fine structure of the synchronization spot is rather stable with respect to the choice of sets of stations included in the analysis.

This implies that reliable precursors should not be expected to exist in the form of simple rises in synchronization; rather they are certain scenarios of developing synchronization [Lyubushin, 2003] including nonmonotonic behavior. As noted in [Sobolev and Lyubushin, 2006, 2007; Lyubushin and Sobolev, 2006], at present we do not clearly understand physical factors responsible for synchronization of variations in microseismic background parameters. One of the most probable causes is intense atmospheric and oceanic processes and their occurrence is not necessarily confined to the vicinity of recording stations: these processes, both synchronizing noise parameters and triggering strong earthquakes, can develop in any region of the Earth. This can account for the far-range synchronization between widely separated stations observed in Figs. 6h and 6i.

CONCLUSIONS

The joint analysis of variations in the argument maximizing the multifractal spectrum of synchronization (the generalized Hurst parameter) estimated in a moving time window 12 h wide for LF microseismic oscillations observed at various IRIS stations has revealed significant effects of synchronization of these variations (coherent behavior) with the help of a multifractal spectrum measure of synchronization. The synchronization measure was estimated in a moving window 5 days wide. The analyzed time intervals immediately preceded the Kronotsky earthquake of December 5, 1997 ($M = 7.8$); the Hokkaido earthquake of September 25, 2005 ($M = 8.3$); and the Simushir, Kurile Islands, earthquake of November 15, 2006 ($M = 8.2$). The respective lengths of the intervals were 30.5, 25, and 61.5 days. The stations included in the analysis were located at epicentral distances of 70 to 7160 km from these earthquakes.

Effects of synchronization of variations in the generalized Hurst parameter at periods of 2.5 h and longer beginning from three to seven days before an event are discovered before the Kronotsky and Hokkaido earthquakes. No synchronization is detected immediately before the Simushir earthquake of November 15, 2006, but a time interval 16 days long (October 11–28, 2006) is revealed that is characterized by coherent behavior of the microseismic noise parameter considered. In all cases, the detected synchronization effects are fairly stable with respect to changes in the set of analyzed stations and the coherence persists even between widely separated stations.

The analysis of synchronization effects of fractal and multifractal parameters of microseismic effects in the range of periods from 1 to 300 min can provide important information on the development process of strong earthquakes; triggering effects resulting in drops of accumulated stresses; and interactions of the lithosphere with oceanic, atmospheric, and ionospheric processes. Further research in this direction should include the use of global information and joint analysis of data (monitoring time series) on the solid and fluid shells of the Earth.

ACKNOWLEDGMENTS

This work was supported by the Presidium of the Russian Academy of Sciences, the program "Electronic Earth"; INTAS, grant no. 05-100008-7889; and the Russian Foundation for Basic Research, project no. 06-05-64625.

REFERENCES

1. J. Berger, P. Davis, and G. Ekstrom, "Ambient Earth Noise: A Survey of the Global Seismographic Network," J. Geophys. Res. **109**, B11307 (2004).
2. D. R. Brillinger, *Time Series. Data Analysis and Theory* (Holt, Rinehart and Winston, New York, 1975; Mir, Moscow, 1980).
3. G. Currenti, C. del Negro, V. Lapenna, and L. Telesca, "Multifractality in Local Geomagnetic Field at Etna Volcano, Sicily (Southern Italy)," Nat. Hazards and Earth System Sci., No. 5, 555–559 (2005).
4. G. Ekstrom, "Time Domain Analysis of Earth's Long-Period Background Seismic Radiation," J. Geophys. Res. **106** (B11), 26 483–26 493 (2001).
5. J. Feder, *Fractals* (Plenum Press, New York, 1988; Mir, Moscow, 1991).
6. A. Friedrich, F. Krüger, and K. Klinge, "Ocean-Generated Microseismic Noise Located with the Gräfenberg Array," J. Seismol. **2** (1), 47–64 (1998).
7. W. Hardle, *Applied Nonparametric Regression* (Cambridge Univ., Cambridge, 1989; Mir, Moscow, 1993).
8. H. E. Hurst, "Long-Term Storage Capacity of Reservoirs," Trans. Amer. Soc. Civ. Eng. **116**, 770–808 (1951).
9. Y. Ida, M. Hayakawa, A. Adalev, and K. Gotoh, "Multifractal Analysis for the ULF Geomagnetic Data during the 1993 Guam Earthquake," Nonlinear Processes in Geophysics **12**, 157–162 (2005).
10. J. W. Kantelhardt, S. A. Zschiegner, E. Konscienly-Bunde, et al., "Multifractal Detrended Fluctuation Analysis of Nonstationary Time Series," Phys. A **316**, 87–114 (2002).
11. N. Kobayashi and K. Nishida, "Continuous Excitation of Planetary Free Oscillations by Atmospheric Disturbances," Nature **395**, 357–360 (1998).
12. D. Kurrle and R. Widmer-Schnidrig, "Spatiotemporal Features of the Earth's Background Oscillations Observed in Central Europe," Geophys. Rev. Lett. **33** (2006).
13. E. M. Lin'kov, *Seismic Phenomena* (LGU, Leningrad, 1987) [in Russian].
14. E. M. Lin'kov, L. N. Petrova, and K. S. Osipov, "Seismogravitational Pulsations of the Earth and Atmosphere Disturbances as Possible Precursors of Strong Earthquakes," Dokl. Akad. Nauk SSSR **313** (5), 1095–1098 (1990).
15. A. A. Lyubushin, "Analysis of Canonical Coherences in the Problems of Geophysical Monitoring," Fiz. Zemli, No. 1, 59–66 (1998) [Izvestiya, Phys. Solid Earth **34**, 52–58 (1998).
16. A. A. Lyubushin, "Wavelet-Aggregated Signal and Synchronous Peaked Fluctuations in Problems of Geophysical Monitoring and Earthquake Prediction," Fiz. Zemli, No. 3, 20–30 (2000) [Izvestiya, Phys. Solid Earth **36**, 204–213 (2000).
17. A. A. Lyubushin, "A Robust Wavelet-Aggregated Signal for Geophysical Monitoring Problems," Fiz. Zemli, No. 9, 37–48 (2002) [Izvestiya, Phys. Solid Earth **38**, 745–755 (2002)].
18. A. A. Lyubushin, "Pulses and Scenarios of Synchronization in Geophysical Observations," in *Essays of Geophysical Research (the 75th Anniversary of the Schmidt United Institute of Physics of the Earth*) (OIFZ RAN, Moscow, 2003), pp. 130–134 [in Russian].
19. A. A. Lyubushin, *Analysis of Data of Geophysical and Ecological Monitoring Systems* (Nauka, Moscow, 2007) [in Russian].
20. A. A. Lyubushin, V. F. Pisarenko, V. V. Ruzhich, and V. Yu. Buddo, "Identification of Periodicities in the Seismic Regime," Vulkanol. Seismol., No. 1, 62–76 (1998).
21. A. A. Lyubushin and G. A. Sobolev, "Multifractal Measures of Synchronization of Microseismic Oscillations in a Minute Range of Periods," Fiz. Zemli, No. 9, 18–28 (2006) [Izvestiya, Phys. Solid Earth **42**, 734–744 (2006)].
22. S. Mallat, *A Wavelet Tour of Signal Processing* (Academic Press, San Diego, 1998; Mir, Moscow, 2005).
23. B. B. Mandelbrot, *The Fractal Geometry of Nature* (Freeman, New York, 1982; Inst. Komp'yut. Issled., Moscow, 2002).
24. S. L. Marple, Jr., *Digital Spectral Analysis with Applications* (Prentice-Hall, Englewood Cliffs, 1987; Mir, Moscow, 1990).
25. D. E. McNamara and R. P. Buland, "Ambient Noise Levels in the Continental United States," Bull. Seismol. Soc. Am. **94**, 1517–1527 (2004).

26. G. Nicolis and I. Prigogine, *Exploring Complexity, an Introduction* (Freedman, New York, 1989; Mir, Moscow, 1990).
27. L. N. Petrova, "Seismogravitational Oscillations of the Earth from Observations by Spaced Vertical Pendulums in Eurasia," Fiz. Zemli, No. 4, 83–95 (2002) [Izvestiya, Phys. Solid Earth **38**, 325–336 (2002)].
28. L. N. Petrova, E. G. Orlov, and V. V. Karpinskii, "On the Dynamics and Structure of Earth's Oscillations in December 2004 from Seismic Gravimeter Observations in St. Petersburg," Fiz. Zemli, No. 2, 12–20 (2007) [Izvestiya, Phys. Solid Earth **43**, 111–118 (2007)].
29. N. K. Pleskach, "Quasi-Harmonic Microseismic Background Oscillations in a Frequency Range of 1–5 Hz," Dokl. Akad. Nauk SSSR **232** (3), 558–561 (1977).
30. A. Ramírez-Rojas, A. Munoz-Diosdado, C. G. Pavia-Miller, and F. Angulo-Brown, "Spectral and Multifractal Study of Electroseismic Time Series Associated to the M_w = 6.5 Earthquake of 24 October 1993 in Mexico," Natural Hazards and Earth System Sci., No. 4, 703–709 (2004).
31. J. Rhie and B. Romanowicz, "Excitation of Earth's Continuous Free Oscillations by Atmosphere–Ocean–Seafloor Coupling," Nature **431**, 552–554 (2004).
32. J. Rhie and B. Romanowicz, "A Study of the Relation between Ocean Storms and the Earth's Hum," Geochem. Geophys. Geosystems, Electronic J. Earth Sci. **7** (10) (2006).
33. L. N. Rykunov, O. B. Khavroshkin, and V. V. Tsyplakov, "Time Variations of High-Frequency Seismic Noise," Izv. Akad. Nauk SSSR, Fiz. Zemli, No. 11, 72–77 (1979).
34. L. N. Rykunov, O. B. Khavroshkin, V. V. Tsyplakov, and N. A. Vidmont, "Modulation of High-Frequency Seismic Noise in Relation to Weak Seismicity of the Earth," Dokl. Akad. Nauk **358** (2), 256–259 (1998).
35. V. A. Saltykov, V. I. Sinitsyn, and V. N. Chebrov, "High-Frequency Seismic Noise from Monitoring in Kamchatka," Fiz. Zemli, No. 3, 39–47 (1997) [Izvestiya, Phys. Solid Earth **33**, 205–212 (1997)].
36. R. Savit and M. Green, "Dependent Variables in Broad Band Continuous Time Series," Physica D **50**, 521–544 (1991).
37. V. B. Smirnov, A. V. Ponomarev, Qian Jiadong, and A. S. Cherepanov, "Rhythms and Deterministic Chaos in Geophysical Time Series," Fiz. Zemli, No. 6, 6–28 (2005) [Izvestiya, Phys. Solid Earth **41**, 428–448 (2005)].
38. G. A. Sobolev, "Microseismic Variations Prior to a Strong Earthquake," Fiz. Zemli, No. 6, 3–13 (2004) [Izvestiya, Phys. Solid Earth **40**, 455–464 (2004)].
39. G. A. Sobolev, A. A. Lyubushin, and N. A. Zakrzhevskaya, "Synchronization of Microseismic Variations within a Minute Range of Periods," Fiz. Zemli, No. 8, 3–27 (2005) [Izvestiya, Phys. Solid Earth **41**, 599–621 (2005)].
40. G. A. Sobolev and A. A. Lyubushin, "Microseismic Impulses as Earthquake Precursors," Fiz. Zemli, No. 9, 5–17 (2006) [Izvestiya, Phys. Solid Earth **42**, 721–733 (2006)].
41. G. A. Sobolev and A. A. Lyubushin, "Microseismic Anomalies before the Sumatra Earthquake of December 26, 2004," Fiz. Zemli, No. 5, 3–16 (2007) [Izvestiya, Phys. Solid Earth **43**, 341–353 (2007)].
42. A. A. Spivak, V. G. Spungin, E. G. Bugaev, and E. M. Gorbunova, "Diagnostic of Tectonic Structures in the Area of the Novo-Voronezhskaya Nuclear Power Plant Based on the Analysis of Microseismic Vibrations," Geoekologiya, No. 3, 268–276 (1999).
43. A. A. Spivak and S. B. Kishkina, "The Use of Microseismic Background for the Identification of Active Geotectonic Structures and Determination of Geodynamic Characteristics," Fiz. Zemli, No. 7, 35–49 (2004) [Izvestiya, Phys. Solid Earth **40**, 573–586 (2004)].
44. L. Stehly, M. Campillo, and N. M. Shapiro, "A Study of the Seismic Noise from Its Long-Range Correlation Properties," J. Geophys. Res. **111**, B10306 (2006).
45. V. N. Tabulevich, *Multidisciplinary Studies of Microseismic Vibrations* (Nauka, 1986) [in Russian].
46. T. Tanimoto, "Continuous Free Oscillations: Atmosphere–Solid Earth Coupling," Annu. Rev. Earth Planet. Sci. **29**, 563–584 (2001).
47. T. Tanimoto, "The Oceanic Excitation Hypothesis for the Continuous Oscillations of the Earth," Geophys. J. Int. **160**, 276–288 (2005).
48. T. Tanimoto, J. Um, K. Nishida, and N. Kobayashi, "Earth's Continuous Oscillations Observed on Seismically Quiet Days," Geophys. Rev. Lett. **25**, 1553–1556 (1998).
49. T. Tanimoto and J. Um, "Cause of Continuous Oscillations of the Earth," J. Geophys. Res. **104**, 723–39 (1999).
50. M. S. Taqqu, "Self-Similar Processes," in *Encyclopedia of Statistical Sciences* (Wiley, New York, 1988), Vol. 8, pp. 352–357.
51. L. Telesca, C. Colangelo, and V. Lapenna, "Multifractal Variability in Geoelectrical Signals and Correlations with Seismicity: A Study Case in Southern Italy," Natural Hazards and Earth System Sci., No. 5, 673–677 (2005).
52. D. L. Turcotte, *Fractals and Chaos in Geology and Geophysics,* 2nd ed. (Univ. Press, New York, 1997).
53. V. N. Zharkov and V. P. Trubitsyn, *Physics of Planetary Interiors* (Nauka, Moscow, 1980) [in Russian].